Journal of Agricultural Research, Development, Extension, and Technology, 2(1), 1-12 (2020)

Full Paper

Evaluation of plant reflectance response with elevation using multispectral images captured by an unmanned aerial vehicle (UAV)

Tito Jun T. Tidula[1], Willie Jones B. Saliling[2] and Renel M. Alucilja[2]

[1]University of Southern Mindanao Agricultural Research Center (USMARC), University of Southern Mindanao, Kabacan, Cotabato, Philippines

[2]Department of Agricultural Biosystems Engineering, College of Engineering and Information Technology, University of Southern Mindanao, Kabacan, Cotabato, Philippines

Received: March 09, 2020
Revised: October 17, 2020
Accepted: November 24, 2020

Abstract

The survival, development and productivity of plants can be affected by elevation. Remote sensing has been used to study altitudinal gradient and plant reflectance. Plant reflectance is an important factor for determining plant health and phenology. This study presents a technique to support a better understanding of how plant reflectance is associated with elevation. In particular, this study determined the effect of elevation on reflectance of pineapple. This study was conducted at Polomolok, South Cotabato, Philippines. The Unmanned Aerial Vehicle (UAV) platform, eBee Ag, onboard the Parrot Sequoia multispectral camera was used to capture multispectral images at 121 meters flight altitude with 80% image overlap on eight areas located at 400-500 meter-above-sea-level (masl) (Location 1) and 650-700 masl (Location 2) elevations. Image stitching was done through Pix4DMapper 3.1 using Ag Multispectral template. The root mean square error (RMSE) for the x-, y- and z- direction justified good and comparable accuracy for all images stitched. Multispectral images captured by an UAV could discriminate plant reflectance response in different elevations. Most of the data demonstrate a moderate positive correlation between elevation and green, red, red-edge and near-infrared reflectance. The only exceptions were correlations between elevation and red-edge reflectance (no correlation), and between elevation and near-infrared reflectance (weak correlation) in Location 2.

Keywords - fixed-wing drone, image processing, multispectral camera, Pix4DMapper, Quantum Geographic Information System (QGIS)

Introduction

Environmental signals dictate plant reaction or response to light, gravity, minerals and water availability. Environmental signals can influence the length, intensity and direction of plant growth, suggesting a complex process that makes plant behavior non-automatic (Trewavas, 2009). Sunlight or spectral characteristics also affect plants' response. Several digital sensors have been developed to measure spectral characteristics. The capability of sensors to quantify environment and plant relations permits us to measure things through remote sensing at flexible scales and precise degree (Adler, 2018).

Satellite and/or point-shot camera are primary platforms for remote sensing, and these have advantages and disadvantages. Satellite imagery may suffer from low spatial resolution, cloud blockage, and other atmospheric effects. Meanwhile, near-surface cameras capture limited scenery, viewing only what is in front of the system, thereby blocking the background vegetation which may cause a false view of the vegetation. These disadvantages are encountered when conducting trials but can be rectified by using a process showing the vegetation at a degree between the satellite and the near-surface camera (Klosterman & Richardson, 2017; Klosterman et al., 2018). The use of an Unmanned Aerial Vehicle (UAV) or drone as another platform for remote sensing observation fills the gap between satellite and near-surface remote sensing. The UAV provides high temporal and spatial resolution (Berra et al., 2016; Kavoosi

Corresponding author email: Tito Jun T. Tidula, tjtidula@usm.edu.ph

et al., 2020; Matese et al., 2015) which is promising for direct reflectance measurement system (Hakala et al., 2018).

A UAV has been considered to be one of the potential equipment for precision agriculture (Daponte et al., 2019) and is commonly used to measure spectral reflectance. Spectral reflectance is one of the characteristics of vegetation and an important tool for studying plant stress physiology (Richardson & Berlyn, 2002) and plants' response to environmental signals (Richardson et al., 2003). In remote sensing, spectral reflectance can be used for weed monitoring, soil water assessment for irrigation, crop monitoring especially for biomass estimates (Peñuelas & Filella, 1998), plant growth (Li et al., 2001) and productivity, health assessment (Ahirwar et al., 2019; Daponte et al., 2019), and identification of actual land use (Honrado et al., 2017). The combination of UAV and spectral reflectance with the use of advanced sensors like the multispectral camera can capture data that the human eye cannot perceive (Veroustraete, 2015) through different spectral wavebands and this can be interpreted to determine the features in the area.

Elevation may dictate the kind of lights that plants are exposed to, the water that plants receive, and the soil nutrients that are available to the plant. With this, some plants live well in low or middle elevations while others thrive in high elevations (McDaniel, 2017). Plants in higher elevation receive more direct sunlight than plants in lower elevation (Gale, 2004; Hakala et al., 2018), but the proportion of days with heavy clouds also increases with elevation (Richardson & Berlyn, 2002). Although plants in higher elevation obtain enough sunlight for their growth, this sunlight has a shortwave radiation (Gale, 2004) which can be damaging to plants when it exceeds the allowable amount (McDaniel, 2017). Lower elevation plants receive safer light since less short-wave radiation reaches farther into these regions (McDaniel, 2017). This supports the statement of Jin et al. (2008) and Zhan et al. (2011) that elevation is an important controlling factor in vegetation growth and contributes a significant influence on the distribution of vegetation. With the elevation effect on plant growth, the spectral characteristics of the plants may also alter. Thus, this study was conducted to determine plant reflectance in varying elevations through the use of UAV.

Materials and Methods

Study Sites and Selection

This study was conducted in pineapple areas in Polomolok, South Cotabato, Philippines (Figure 1). The area has Type IV climate characterized with more or less evenly distributed rainfall throughout the year (Elegado et al., 2016). Plant uniformity, plant variety, and difference in elevation were considered in area selection. Plants in this study were at the canopy closure stage, 270-300 days

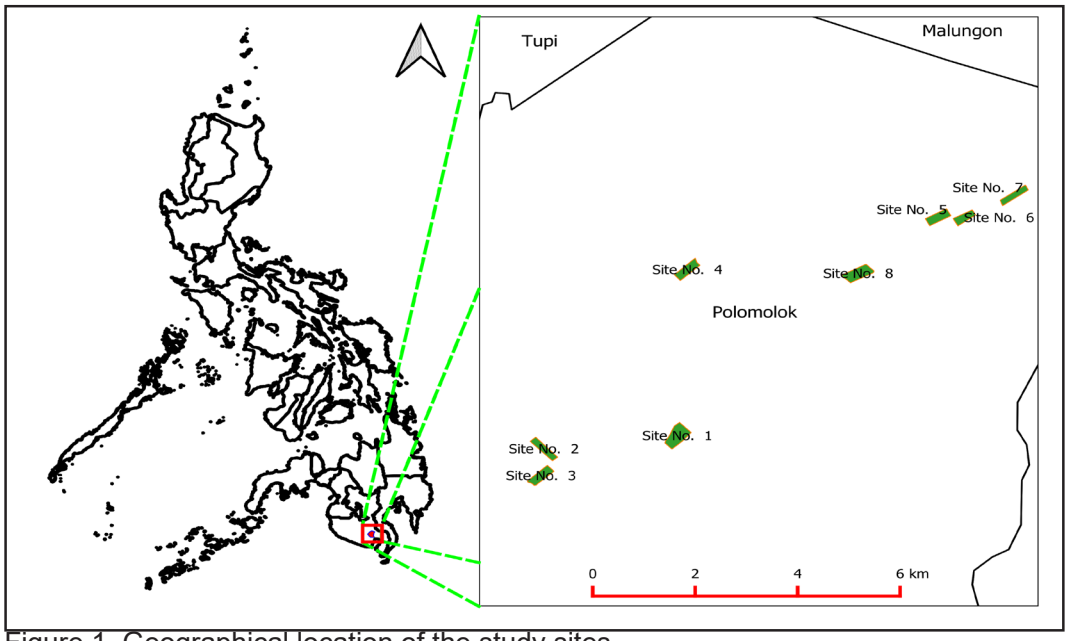

Figure 1. Geographical location of the study sites.

after planting. At canopy closure stage, the soil is fully covered with plant leaves, thus eliminating possible reflectance from the soil. Plant stage was the same in all study sites characterized by erect leaves with light green to dark green leaf color. Two elevation range groups were selected: one at 400-500 meter-above-sea-level (masl) (Location 1) and the other at 650-700 masl (Location 2). The data plot approximately covered five hectares in each study location.

UAV Platform and Multispectral Camera Used

The eBee Ag, a fixed-wing UAV platform, onboard the Parrot Sequoia Multispectral Camera (Parrot Sequoia MSP) and sunshine sensor were used to obtain plant reflectance and the digital surface model (DSM) of the study area. The eBee Ag (developed by senseFly SA: A Parrot Company, Switzerland) was made from ultralight materials (700 g) and can be used and adjusted on a preferred setting. Compatible with it is the Parrot Sequoia multispectral camera (developed by the Parrot SA, Paris, France) containing four separate spectral sensors and one RGB sensor with image resolution of 1280x960 and 3264x4896 pixels, respectively.

The Parrot Sequoia MSP captured green, red, red-edge and near-infrared (NIR) spectral reflectance with center wavelength of 550, 660, 735, and 790 nm, and bandwidth of 40, 40, 10, and 40 nm, respectively. A sunshine sensor was mounted to the multispectral camera to measure the incoming solar radiation with four sensors and had the same band as the Parrot Sequoia MSP. The data captured by the sunshine sensor was used to calibrate and normalize the images, and made it possible to compare photos over time despite variations in light during photo shoots.

Flight Planning and Aerial Imaging Campaign

The plot size for each location was five hectares. To ensure good image overlap on the data plots, aerial imaging was conducted within 20-30 hectares such that the data plot was at the center of the selected area. The UAV flight mission was planned with 80% overlap using the eMotion, a package software that allows the interactions of the operator to the eBee Ag. The eBee Ag flight altitude was maintained at 121 m above ground level (AGL), resulting in ground resolution of approximately 11.4 cm pixel^{-1}. Simultaneously, the Parrot Sequoia MSP took photos every 21.9 m advance flight distance while the distance between flight tracks was 29.2 m. Aerial imaging was conducted from February to March 2019. Imaging time was between 07:00-09:30 AM (Table 1) to ensure that pineapple leaves were already dried, eliminating the possible reflectance contamination from dew. During each aerial imaging campaign, the weather was good and the light was not constantly changing. There were clear to partly cloudy skies with no rolling clouds, guaranteeing that images do not develop deep shadows and sunspots. The deep shadows could significantly affect the multispectral results while the sunspots would produce bright sunspots in the captured images (MicaSense, 2017a).

Table 1 also shows the aerial imaging details per site with the corresponding images captured on four bands. Six flights were conducted to cover the eight sites and took a total of 5,576 raw images that represented approximately 29.62 GB of information. The wind velocity during aerial imaging ranged from 0.4-6.5 ms^{-1} which was lower than the maximum recommended value of 7 ms^{-1} to capture good imagery while maintaining the flight altitude to 121 m AGL at 80% image overlap.

Flight coverage is defined as the ground boundary set during the flight with the corresponding flight altitudes. Increasing area of coverage, numbers of flight lines and/or wind velocity simultaneously influences flight duration. Flight altitude alone has its own effect on the number of captured images and flight duration. Increase in flight altitude decreases the number of images but increases the area covered per image (Mesas-Carrascosa et al., 2015; Torres-Sánchez et al., 2013). In contrast, increase in flight altitude decreases the flight duration with the same flight coverage (Seifert et al., 2019; Torres-Sánchez et al., 2013). Flight duration is also affected by flight coverage and wind velocity (Holy Stone, 2019; Torres-Sánchez et al., 2013). In this study, the number of images increased with flight coverage having the same flight altitude and image overlap.

Before each flight mission, the Parrot Sequoia MSP took the photo of the calibrated reflectance panel (CPR) – AirinovAircalib. The CPR measured the lighting conditions at the time of image capture and represented the actual light reaching the grounds (MicaSense, 2017b), thus creating a reflectance-compensated output by converting

Table 1. Aerial imagery details and the total number of images gathered per flight.

Location No.	Site No.	Flight					Wind Velocity (ms^{-1})	Total Images (4 Band)
		Date	Time (AM)	Duration (min)	Lines	Coverage (ha)		
1	1	2/21/2019	07:13 -07:32	19	12	30	4.4 - 5.4	752
	2 3	2/23/2019	07:09 -07:32	24	19	67	0.4 - 0.6	1308
2	4	2/23/2019	08:13 -08:25	12	9	30.5	1.0 - 1.5	752
	5 6	2/23/2019	09:02 -09:24	22	17	54	1.4 - 2.2	1384
	7	2/28/2019	07:55 -08:06	11	7	27.3	4.3 - 6.5	436
	8	3/14/2019	08:48-09:06	14	14	48.2	1.2 - 2.6	944

the raw pixel values into reflectance (MicaSense, 2017c) during image stitching.

Image Processing

Log and raw imagery (multispectral and RGB images) extraction from the eBee Ag drone and Parrot Sequoia Multispectral Camera took approximately 30 min for each imagery campaign using the eMotion "flight data manager" features. Six flights took a total of 180 min. The data extraction output is a Pix4D project of multispectral raw imagery. During data extraction, the eMotion was able to match the information (coordinates, orientation and altitude) from the drone and the images of the camera to have an accurate and good quality processed orthomosaic.

Image processing and stitching were done using the Pix4Dmapper 3.1 software and the "Ag Multispectral" template (Pix4DMapper, 2016) to produce the Digital Surface Model (DSM) and the reflectance map. The resulting DSM displayed continuous surface features of objects and structures, and was converted into the Digital Terrain Model (DTM) that represented the actual terrain removing the ground-based objects in the Pix4D workflow. The DTM was used in data analysis and interpretation.

Pix4Dmapper Pro 3.1 computed keypoints in each image and used them to find matches between images during initial processing. From the matches, the software iteratively ran a number of automatic aerial triangulation-bundle block adjustment (AAT-BBA) and camera self-calibration steps until best rebuilding was achieved. Georeferencing was done by introducing the camera coordinates in the AAT-BBA stage (Fernández-Guisuraga et al., 2018). Likewise, 11.4 cm $pixel^{-1}$ spatial resolution during image acquisition was re-sampled into 12 cm $pixel^{-1}$ to lower the space requirement of the processing and output orthomosaic. Next, densified point clouds were generated to obtain a highly detailed DSM that was used to produce reflectance maps. The camera and sun irradiance radiometric correction and calibration were applied. Normalization and radiometric corrections were introduced considering the camera parameters written in the EXIF metadata related to the camera (vignetting, dark current, ISO, etc.) and sun irradiance information written in the XMP file (Pix4DMapper, 2016; Adler, 2018; Fernández-Guisuraga et al., 2018). Per band, the AirinovAircalib calibrated reflectance panel (CRP) reflectance values were extracted and the values were used to convert raw pixel data into reflectance values as the latter represented the amount of light reaching the ground during image acquisition.

Since Pix4Dmapper Pro 3.1 processing steps need a large number of computational resources that grow exponentially as more images are simultaneously processed (Fernández-Guisuraga et al., 2018), the software was installed in a high-end computer with Intel(R) Xeon(R) CPU X5570 @ 2.93 GHz processor with 48GB RAM, 64-bit Windows 10 Pro operating system, processing desktop. The

multispectral orthomosaicing took 1783.48 min (29.73 hr). Depending on the area of coverage, the AAT-BBA and camera calibration processing took 9-77 min (0.15-1.5 hr) while point densification and orthomosaic production of the reflectance maps took 25-475 min (0.42-7.92 hr).

Relative Accuracy Determination of the UAV Produced DTM

In the absence of high grade GPS instrument to measure ground control points, the results were validated by determining its relevancy to the Aster DEM (downloaded from https://earthexplorer.usgs.gov). Fifty points were randomly plotted in the data plot. The elevation coincides with the points extracted in the UAV-produced and satellite-based DTM. Relative accuracy was measured through the root mean square error (RMSE).

The relative accuracy was found to be of 0.88 m. This result implies that the UAV-based or the satellite-based (aster) DTM may differ with each other by approximately 0.88 m, which is within the acceptable range.

Data Extraction and Analysis

The DTM and reflectance map were loaded to the Quantum Geographic Information System (QGIS), a free and open source Geographic Information System (GIS) software, installed in a PC with Intel(R) Core(TM) i7-7700 CPU @ 3.60GHz processor with 16.0 GB RAM in a 64-bit Windows 10 Operating System (OS). A polygon vector layer (data plot) separating the road network and other non-pineapple area from the pineapple field was digitized. Using the "clipper" feature of the QGIS, the pineapple area was separated from the road network and other non-pineapple area on the digital terrain model (DTM) and the reflectance map. Using the QGIS vector random-points algorithm, 10,000 randomly plotted points inside the 5-ha polygon were set. The reflectance and elevation model data coinciding with the points were extracted using the Point Sampling in QGIS algorithm. This gave a huge amount of extracted data for better analysis. Outliers ranging from 0.5-3.0% of the total populations were analyzed using interquartile range (IQR). The highest number of outliers was observed in NIR band of Location 2 while the lowest was in the red-edge of both locations. The relationship between reflectance and elevation was quantified using a regression model.

Results and Discussion

Raw Imagery Dataset

Upon examination of raw images gathered, no image anomaly/noise had been observed. Figure 2 shows one of the reflectance photos taken from the third flight. With the color contrast, the difference between vegetation and non-vegetation per band was distinct. Depending on the spectral band, the vegetation reflectance may be lighter or darker compared to the non-vegetative objects. Features like soil, trees and buildings were distinct. For instance, a sandy gully shown as a light-colored band on the upper portion of each image can be easily recognized. The high soil reflectance may be attributed to the moisture content, soil texture, surface roughness, and organic matter component (Ben-dor et al., 2014; Cierniewski & Kuśnierek, 2010; Jain & Singh, 2003; Mzuka et al., 2015; Navalgund, 2002; Stamatiadis et al., 2005). The mentioned soil characteristics are complex, variable and interrelated in view of the reflectance. For example, the presence of moisture on soil will decrease the reflectance especially in visible regions (Cierniewski & Kuśnierek, 2010; Lobell & Asner, 2002; Navalgund, 2002). The soil moisture content is interrelated to soil texture. To mention, coarse sandy soils are usually well-drained, resulting in low moisture content and relatively high reflectance. Otherwise, poorly drained fine textured soils generally have lower reflectance (Lobell & Asner, 2002). Buildings and other infrastructure showed higher reflectance compared to vegetation. This study revealed the potential of using reflectance as a tool for discriminating surface features in different elevations.

Multispectral Image Processing and Output Quality

During initial processing, the 3D reconstruction algorithm (AAT-BBA and camera self-calibration) obtained 100% images alignment on all channels (green, red, red-edge and NIR) on the basis of more than 10,000 keypoints extracted for each image, with over 5,500 keypoints matching adjacent fields. The number of 2D keypoints is shown in Table 2. A high precision in 2D keypoints was observed. The 2D keypoints result indicates that processed images had enough visual contexts. Quality calibration results required at least 1,000 matches per image and this was obtained in this study. From 2D points, the 3D point was computed considering the camera

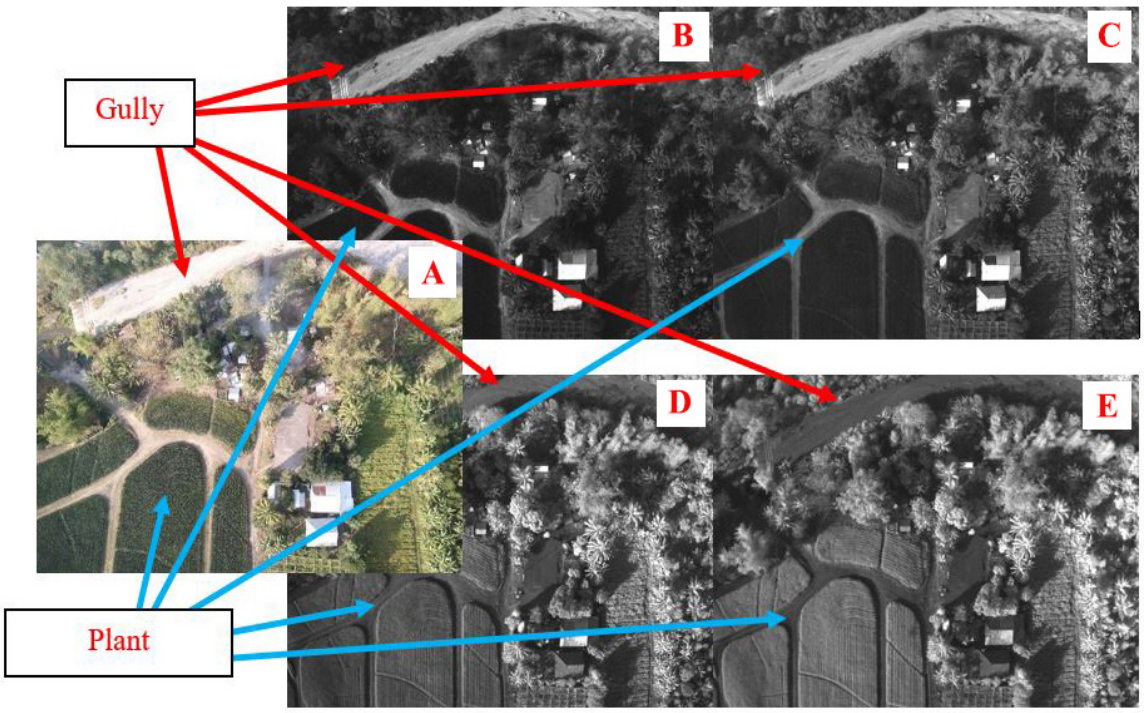

Figure 2. Reflectance raw images captured by Parrot Sequoia Multispectral Camera: (A) RGB image, (B) green band (center wavelength (CW): 550nm, Band Width (BW): 40 nm), (C) red band (CW: 660, BW: 40), (D) red-edge (CW: 735, BW: 10), and (E) NIR (CW: 790, BW: 40).

external and internal parameters and reprojected images for more accurate results. The difference in image projection at 2D and 3D points was represented by the reprojection error. The number of 3D keypoints and the reprojection error are shown in Table 2. During multispectral image processing, higher 3D points and lower reprojection errors indicate higher output accuracy (Pix4D, n.d). The high precision result obtained in this study was due to large forward and side images overlap provided in the keypoints matching process between adjoining images (Dandois et al., 2015; Frey et al., 2018; Santesteban et al., 2017; Seifert et al., 2019; Torres-Sánchez et al., 2018).

The precision of georeferenced images was reported on Pix4D as the root RMSE (Table 3). The RMSE in three directions were comparable across all eight sites and were lower than the Ground Sampling Distance (GSD) which was 11.4 cm pixel^{-1}; thus, the RMSE justified the good and comparable accuracy for the x-, y- and z- direction of stitched images (Pix4D, 2018).

Extracted Data and its Characteristics

The elevation characteristic of the study area is presented in Table 4. The lowest and highest elevations for Location 1 and Location 2 ranged from 419.49-470.23 and 661.20-704.42 masl, respectively. The elevation data were extracted from the DTM which formed part of the product in image processing at Pix4DMapper.

A very low reflectance was observed in the visible region (green and red) in both locations (Table 5). High reflectance was observed in the infrared region which conformed to the findings of Hakala et al. (2018), Roy (1989), and Shafri and Hamdan (2009). Within the visible region reflectance, green reflectance was observed to be higher than red reflectance, which is consistent with previous reports (DigitalGlobe, 2010; Roy, 1989). The low reflectance on red portion can be explained by strong chlorophyll absorbance (Bhandari et al., 2012; DigitalGlobe, 2010; Everitt et al., 1985; Thomas & Gausman, 1977; Turrel et al., 1961; Weichelt et al. n.d) during photosynthetic activity (Roy, 1989). By contrast, most of the green was reflected, which is also the

Table 2. Resulting 2D and 3D keypoints during initial image processing at Pix4DMapper and their reprojection error.

Location No.	Site No.	Flight No.	No. of 2D keypoints	No. of 3D keypoints	Mean Reprojection Error (pixels)
1	1	1	951,389	326,109	0.246
	2	2	1,641,314	587,183	0.248
	3				
2	4	3	833,814	291,133	0.291
	5	4	1,422,961	515,731	0.288
	6				
	7	5	644,667	214,610	0.285
	8	6	905,548	321,923	0.305

Table 3. Computed root mean square error (RMSE) using UAV's GPS location to each georeferenced images in centimeter.

Location No.	Site No.	Flight No.	X	Y	Z
1	1	1	0.42	0.38	0.60
	2	2	0.49	0.36	0.86
	3				
2	4	3	0.48	0.40	0.78
	5	4	0.50	0.32	0.72
	6				
	7	5	0.44	0.41	0.67
	8	6	0.39	0.39	0.70
		p-value	0.506	0.709	0.884

Table 4. Elevation profile of the selected sites in meter-above-sea-level

Location No.	Site No.	Minimum (m)	Maximum (m)	Mean (m)	Standard Deviation
1	1	459.37	470.23	465.11	2.12
	2	447.75	467.47	457.50	4.38
	3	419.49	445.74	433.71	7.29
2	4	655.84	673.29	664.42	3.73
	5	665.96	686.42	678.67	3.68
	6	661.20	673.72	667.70	2.64
	7	665.35	680.14	674.02	3.25
	8	687.05	704.42	687.05	3.66

reason for the leaf's color (Jain & Singh, 2003).

The leaf structure could cause the strong reflection in the infrared portion (Bhandari et al., 2012; Weichelt et al., n.d). The reflectance of red-edge was found to be between that of the red and near-infrared bands. Red-edge value was typically higher than red but lower compared to the near infrared due to the combination effect of chlorophyll content and structure of the leaf (Curran et al., 1990; Weichelt et al., n.d). Nevertheless, healthy plants have low reflectance in the visible region but higher reflectance in the red-edge and infrared band (Navalgund, 2002; Roy, 1989; Shafri & Hamdan, 2009).

Relationship of Reflectance and Elevation

Table 6 shows that all r-values were in the range 0.47-0.64, except for the red-edge and near-infrared reflectance in Location 2 where r = 0.04 and 0.39, respectively. Thus, most values suggest a moderate positive correlation between elevation and reflectance in both locations, except for the relationship between elevation and red-edge in Location 2 where no correlation was observed and between elevation and near-infrared reflectance was weak.

Figure 3 shows the model fitness of pineapple reflectance and the elevation through the coefficient of determination (R^2), which represents the proportion of the variance in reflectance that can be explained by elevation. Among all the spectral reflectance, the data shows that elevation predicts the red reflectance best—33.63% and 40.74% for Locations 1 and 2, respectively.

This study shows an increasing linear trend of reflectance in most bands with the increase of

Table 5. Minimum, maximum and mean reflectance value of pineapple taken by the Parrot Sequoia MSP.

Location No.	Reflectance	Minimum	Maximum	Mean	Standard Deviation
1	Green	0.03	0.07	0.05	0.01
	Red	0.01	0.04	0.02	0.01
	Red-edge	0.11	0.44	0.28	0.06
	NIR	0.23	0.73	0.48	0.09
2	Green	0.03	0.08	0.05	0.01
	Red	0.01	0.05	0.03	0.07
	Red-edge	0.12	0.37	0.25	0.04
	NIR	0.32	0.57	0.45	0.05

Table 6. Results of the regression analysis for each of the four spectral bands in the two locations.

Location No.	Reflectance	Population		ß	*r*	*p*
		Initial	Final*			
1	Green	30,000	29,345	0.0003	0.4683	0.001
	Red	30,000	29,411	0.0002	0.5799	0.001
	Red-edge	30,000	29,849	0.0022	0.5502	0.001
	NIR	30,000	29,345	0.0031	0.4941	0.001
2	Green	50,000	48,829	0.0005	0.6347	0.001
	Red	50,000	49,480	0.0004	0.6383	0.001
	Red-edge	50,000	49,708	0.0001	0.0415	0.001
	NIR	50,000	48,456	0.0016	0.3914	0.001

Note: *Final population after removal of outliers. This data was used in generation of regression model.

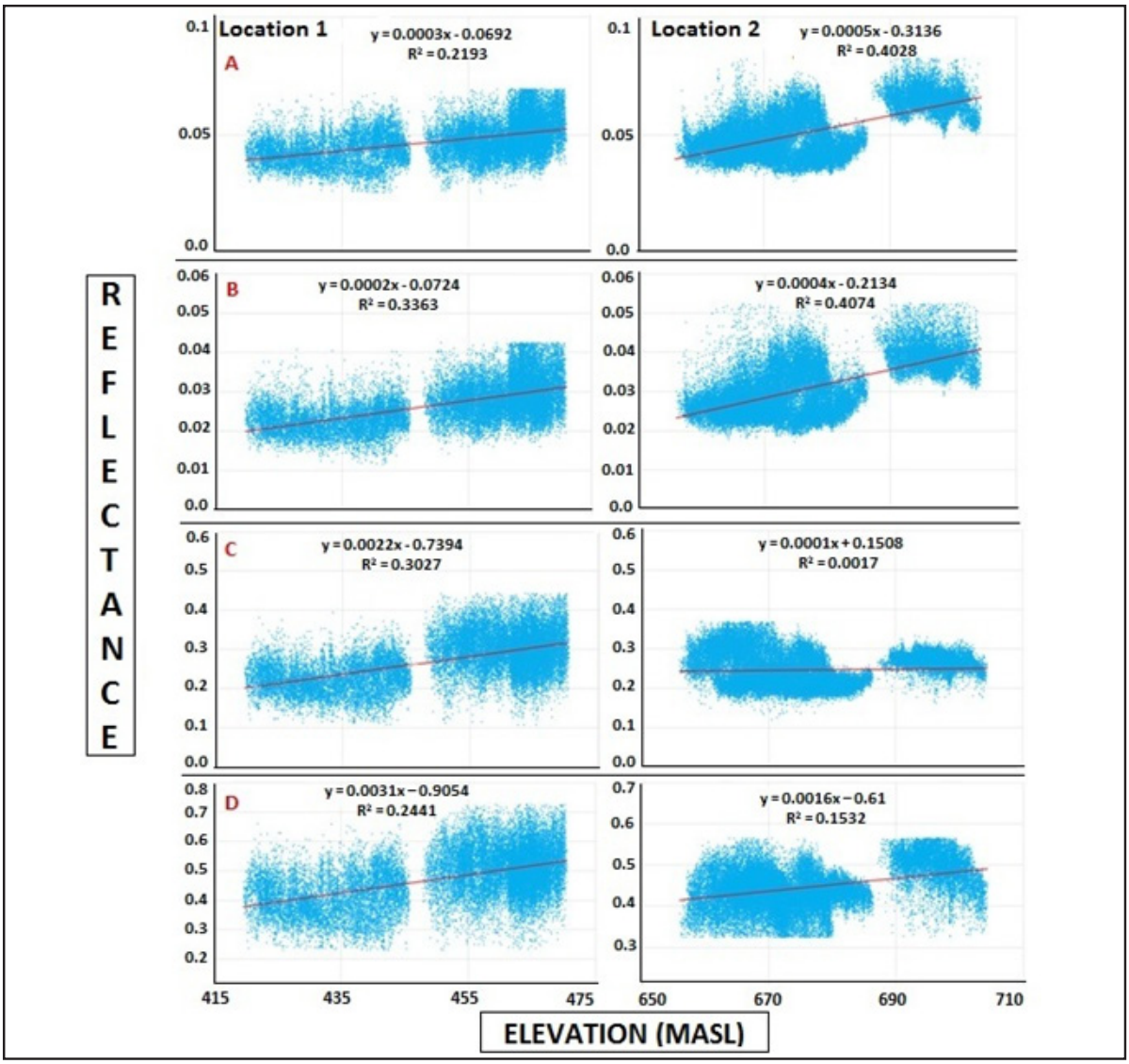

Figure 3. Location 1 and 2 reflectance-elevation plot of four spectral band captured by Parrot Sequoia MSP: (A) green, (B) red, (C) red-edge and (D) near-infrared (NIR). Note: Scales are different across graphs.

elevation, and that this result was validated in two different sites (Location 1 and Location 2). The results confirm those by Richardson et al. (2003) who measured plant reflectance using a UniSpec spectral analysis system (PP Systems, Haverhill, MA). A possible reason why elevation affects reflectance is because of photosynthesis reduction that is associated with a decrease of light absorbance and an increase in reflectance. In turn, this may cause variability in plant physiology processes (Richardson & Berlyn, 2002). Incidentally, an increasing linear trend in reflectance was also found using Landsat 8 imagery in non-organic material such as glaciers found in Western China (Li et al., 2017).

Conclusions

This study showed the usefulness of eBee Ag onboard in UAV with the Parrot Sequoia Multispectral Camera, as remote sensing platform in agricultural research undertakings. Aerial imaging at the maximum wind speed of 6.5 ms^{-1} captured high quality multispectral images free from noise. The data acquisition with 80% overlap produced high precision result at 2D and 3D keypoints during orthomosaicing resulting to good image alignment. Previous studies showed that multispectral images made it possible to discriminate between vegetative and non-vegetative features. This study showed how the same technique can be used to analyze

reflectance at varying elevations, leading to the finding that pineapple reflectance increased with elevation. Most of the data show a moderate positive correlation between elevation and reflectance. Thus, plant reflectance must also consider elevation data for meaningful and precise remotely-sensed data of plant health and phenology.

Disclosure Statement

No potential conflict of interest was reported by the authors.

References

Adler, K. (2018). *Radiometric correction of multispectral images collected by a UAV for phenology studies*. Master's Thesis, Lund University.

Ahirwar, S., Swarnkar, R., Bhukya, S., & Namwade, G. (2019). Application of drone in agriculture. *International Journal of Current Microbiology Applied Sciences*, 8(1), 2500-2505.

Ben-Dor, E., Irons, J., & Epema, G.F. (1999). *Soil reflectance*. Retrieved March 24, 2020 from https://www.researchgate.net/publication/200458942_Soil_Reflectance.

Berra, E.F., Gualto, R., & Barr, S. (2016). *Use of digital camera onboard a UAV to monitor spring phenology at individual tree level.* Beijing, 2016. New Jersey: IEEE.

Bhandari, A.K., Kumar, A., & Singh, G.K. (2012). Feature extraction using normalized difference vegetation index (NDVI): A Case Study of Jabalpur City. *Procedia Technology*, 6. 612-621.

Cierniewski, J. & Kuśnierek, K. (2010). Influence of several size properties on soil surface reflectance. *Quaestiones Geographicae*, 29(1), 13-25. Adam Mickiewicz University Press, Poznań.

Curran, P.J., Dungan, J.L., & Gholz, H.L. (1990). Exploring the relationship between reflectance red edge and chlorophyll content in slash pine. *Tree Physiology*, 7, 33-48.

Dandois, J.P., Olano, M., & Ellis, E.C. (2015). Optimal altitude, overlap, and weather conditions for computer vision UAV estimates of forest structure. *Remote Sensing, 7,* 13895-13920.

Daponte, P., De Vito, L., Glielmo, L., Iannelli, L., Liuzza, D., Picariello, F., & Silano, G. (2019). A review on the use of drones for precision agriculture. *IOP Conf. Series: Earth and Environmental Science*, 275. DOI:10.1088/1755-1315/275/1/012022

Digital Globe (2010). Whitepaper: The benefits of the eight spectral bands of worldview-2. Retrieved July 23, 2018 from https://dg-cms-uploads-production.s3.amazonaws.com/uploads/document/file/35/DG-8SPECTRAL-WP_0.pdf

Elegado, F., Colegio, S., Lim, V., Gervasio, A., Perez, M., Balolong, M., Banaay, C.G., & Mendoza, B. (2016). Ethnic fermented foods of the Philippines with reference to lactic acid bacteria and yeasts. In J. P. Tamang (Ed.) Ethnic fermented foods and alcoholic beverages of Asia (pp. 323-340). New Delhi: Springer.

Everitt, J.H., Richardson, A.J. & Gaussman, H.W. (1985). Leaf reflectance-nitrogen-chlorophyll relations in buffelgrass. *Photogrammetric Engineering Remote Sensing*, 51, 463-466.

Fernández-Guisuraga, J.M., Sanz-Ablanedo, E., Suarez-Seoane, S., & Calvo, L. (2018). Using unmanned aerial vehicle in postfire vegetation survey campaigns through large and heterogeneous areas: opportunities and challenges. *Sensors*, 18, 586.

Frey, J., Kovach, K., Stemmler, S., & Koch, B. (2018). UAV photogrammetry of forests as a vulnerable process. A sensitivity analysis for a structure from motion RGB-Image pipeline. *Remote Sensing*, 10, 912.

Gale, J. (2004). Viewpoint: Plants and altitude-revisited. *Annals of Botany*, 94, 199.

Hakala, T., Markelin, L., Honkavaara, E., Scott, B., Theocharous, T., Nevalainen, O., Nasi, R., Suomalainen, J., Viljanen, N., Greenwell, C., & Fox, N. (2018). Direct reflectance measurements from drones: sensor absolute radiometric calibration and system tests for forest reflectance characterization. *Sensors*, 18, 1417.

Holy Stone (2019). 5 factors affect the flight time of drones. Retrieved March 25, 2020 from http://www.holystone.com/en/blog/FlyingFun/FlightTime.html

Honrado, J.L.E., Solpico, D.B., Favila, C.M., Tongson, E., Tangonan, J.L., & Libatique, N.J.C. (2017). UAV imaging with low-cost multispectral imaging system for precision agriculture applications. Retrieved September 14, 2020 from https://www.researchgate.net/publication/322058876 with DOI: 10.1109/GHTC.2017.8239328

InfoAg (2016). Paul Spaur (Pix4D) - Real data, real results. St. Louis, MO. Retrieved September 13, 2017 from https://infoag.org/presentations/2407.pdf.

Jain, S.K. & Singh, V.P. (2003). Water resources systems planning and management. Amsterdam, the Netherlands: Elsevier. Retrieved December 3, 2020, from https://webapps.unitn.it/Biblioteca/it/Web/EngibankFile/5414341.pdf.

Jin, X.M., Zhang, Y.-K., Schaepan, M.E., Clevers, J.G.P.W., & Su, Z. (2008). Impact of elevation and aspect on the spatial distribution of vegetation in the Qilian mountain area with remote sensing data. *The International archives of the Photogrammetry, Remote Sensing and spatial Information Sciences*, Beijing., 37, 1385-1390.

Kavoosi, Z., Raoufat, M.H., Dehghani, M., Jafari, A., Kazemeini, S.A., & Nazemossadat, M.J. (2020). Feasibility of satellite and drone images for monitoring soil residue cover. *Journal of the Saudi Society of Agricultural Sciences*, 19. 56-64.

Klosterman, S., Melaas, E., Wang, J.A., Martinez, A., Frederick, S., O'Keefe, J., & Richardson, A.D. (2018). Fine-scale perspectives on landscape phenology from unmanned aerial vehicle phenology. *Agricultural and Forest Meteorology*, 248, 397-407.

Klosterman, S. & Richardson, A.D. (2017). Observing spring and fall phenology in a deciduous forest with aerial drone imagery. *Sensors*, 17,1-17.

Li, H., Lascano, R., Barnes, E., Booker, J., Wilson, T., Bronson, K., & Segarra, E. (2001). Multispectral reflectance of cotton related to plant growth, soil water and texture, and site elevation. *Agronomy Journal*, 19, 1327-1337.

Li, X., Wu, W., Xu, B., Yin, S., Yang, R., & Cheng, S. (2017). Reflectance-elevation relationship and their seasonal patterns over twelve glaciers in western China based on Landsat 8 data. *Remote Sensing*, 9, 187.

Lobell, D.B. & Asner, G. (2002). Moisture effects on soil reflectance. *Soil Science Society of America Journal.* 66. 722-727. DOI:10.2136/sssaj2002.7220.

Matese, A., Toscano, P., Di Gennaro, S.F., Genesio, L., Vaccari, F.P., Primicerio, J., Belli, C., Zaldei, A., Bianconi, R., & Gioli, B. (2015). Intercomparison of UAV, aircraft and satellite remote sensing platforms for precision viticulture. *Remote Sensing*, 7, 2971-2990.

McDaniel, J. (2017). How does altitude affect vegetation. Retrieved December 26, 2018 from https://www.hunker.com/12003620/how-does-altitude-affect-vegetation

Mesas-Carrascosa, F.J., Torres-Sánchez, J., Clavero-Rumbao, I., Garciá-Ferrer, A., Peña, J.M., Borra-Serrano, I., & López-Granados. (2015). Assessing optimal flight parameters for generating accurate multispectral orthomosaicks by UAV to support site-specific crop management. *Remote Sensing*, 7. 12793-12814.

MicaSense. (2017a, December 20). Best practices: Collecting data with MicaSense RedEdge and Parrot Sequoia - MicaSense knowledge base. Support MicaSense. Retrieved June 23, 2017 from https://support.micasense.com/hc/en-us/articles/224893167-Best-practices-Collecting-Data-with-MicaSense-RedEdge-and-Parrot-Sequoia

MicaSense. (2017b, November 22). How do calibrated reflectance panels improve my data? - MicaSense knowledge base. Support MicaSense. Retrieved June 23, 2017 from https://support.micasense.com/hc/en-us/articles/220154947-How-do-calibrated-reflectance-panels-improve-my-data

MicaSense. (2017c, July 25). Use of calibrated reflectance panels for rededge data - MicaSense knowledge base. Support MicaSense. Retrieved December 23, 2018 from https://support.micasense.com/hc/en-us/articles/115000765514-Use-of-Calibrated-Reflectance-Panels-For-RedEdge-Data.

Mzuka, M., Khosla, R., & Reich, R. (2015). Bare soil reflectance to characterize variability in soil properties. *Communications in Soil Science and Plant Analysis*, 46, 1668-1676.

Navalgund, R. (2002). Remote sensing. *Resonance*, 6, 51-60.

Pix4D. (2018). Do more GCPs equal more accurate drone maps?. Retrieved March 26, 2020, from https://www.pix4d.com/blog/GCP-accuracy-drone-maps

Pix4D. (n.d). Quality Report Help. Retrieved March 25, 2020, from https://support.pix4d.com/hc/en-us/articles/202558689-Quality-Report-Help#label100

Pix4DMapper. (2016). Pix4Dmapper 3.1: User Manual. Pix4d SA. 1015 Lausanne, Switzerland.

Richardson, A.D. & Berlyn, G.P. (2002). Spectral reflectance and photosynthetic properties of *Betula papyrifera* (Betulaceae) leaves along an elevational gradient on Mt. Mansfield, Vermont, USA. *American Journal of Botany*, 89, 88-94.

Richardson, A., Berlyn, G., & Duigan, S. (2003). Reflectance of Alaskan black spruce and white spruce foliage in relation to elevation and

latitude. *Tree Physiology*, 23, 537-544.

Roy, P.S. (1989). Spectral reflectance characteristics of vegetation and their use in estimating productive potential. Proceedings Indian Academy Sciences (Plant Sciences), 99, No., 59-81.

Santesteban, L.G., Di Gennaro, S.F., Herrero-Langreo, A., Miranda, C., Royo, J.B., & Matese, A. (2017). A high resolution UAV-based thermal imaging to estimate the instantaneous and seasonal variability of plant water status within vineyard. *Agricultural Water Management,* 183, 49-59.

Seifert, E., Seifert, S., Vogt, H., Drew, D., van Aardt, J., Kunneke, A., & Seifert, T. (2019). Influence of drone altitude, image overlap, and optical sensor resolution on multi-view reconstruction of forest images. *Remote Sensing*, 11, 1252.

Shafri, H.Z.M. & Hamdan, N. (2009). Hyperspectral imagery for mapping disease infection in oil palm plantation using vegetation indices and red edge techniques. *American Journal of Applied Sciences*, 6, 1031-1035.

Stamatiadis, S., Christofides, C., Tsadilas, C., Samaras, V., Schepers, J.S., & Francis, D. (2005). Ground-sensor soil reflectance as related to soil properties and crop response in a cotton field. *Precision Agriculture*, 6, 399-411.

Thomas, J.R. & Gausman, H.W. (1977). Leaf reflectance vs. leaf chlorophyll and carotenoid concentrations for eight crops. *Agronomy Journal*, 69, 799-811.

Torres-Sánchez, J., López-Granados, F., Borra-Serrano, I., & Peña, J.M. (2018). Assessing UAV-collected image overlap influence on computation time and digital surface model accuracy in olive orchards. *Precision Agriculture*, 19, 115-133.

Torres-Sánchez, J., López-Granados, F., De Castro AI, Peña-Barragán, J.M. (2013) Configuration and specifications of an unmanned aerial vehicle (UAV) for early site specific weed management. *PLoS One* 8(3), e58210.

Trewavas, A. (2009). What is plant behaviour?. *Plant, Cell and Environment*, 32, 606-616.

Veroustraete, F. (2015). The rise of the drones in agriculture. *EC Agriculture*, 2, 325-327.

Weichelt, H., Rosso, P., Marx, A., Reigber, K.M., & Heynen, M. (n.d.).The rapid eye red edge band (White Paper). Retrieved June 23, 2018, from https://resa.blackbridge.com/files/2014-06/Red_Edge_White_Paper.pdf

Zhan, Z., Liu, H., Li, H., Wu, W., & Zhong, B. (2011). The relationship between NDVI and terrain factors - a case study of Chongqing. *Procedia Environmental Science*, 12B, 765-771.